Solid State Experiments at High Pressure and Strain Rates

D.H. Kalantar, B.A. Remington, J.D. Colvin,
K.O. Mikaelian, S.V. Weber, L.G. Wiley, J.S. Wark,
A. Loveridge, A.M. Allen, A. Hauer, M.A. Meyers

November 24, 1999

U.S. Department of Energy

Lawrence
Livermore
National
Laboratory

Solid state experiments at high pressure and strain rates*

D. H. Kalantar, B. A. Remington, J. D. Colvin, , K. O. Mikaelian, S. V. Weber, L. G. Wiley

Lawrence Livermore National Laboratory, Livermore California 94550

J. S. Wark, A. Loveridge, A. M. Allen

Department of Physics, Clarendon Laboratory, University of Oxford, Oxford, OX1 3PU

A. Hauer

Los Alamos National Laboratory, Los Alamos, New Mexico 87545

M. A. Meyers

University of California at San Diego, La Jolla, California 92093

Experiments have been developed using high powered laser facilities to study the response of materials in the solid state under extreme pressures and strain rates. Details of the target and drive development required for solid state experiments and results from two separate experiments are presented. In the first, thin foils were compressed to a peak pressure of 180 GPa and accelerated. A pre-imposed modulation at the embedded RT unstable interface was observed to grow. The growth rates were fluid-like at early time, but suppressed at later time. This result is suggestive of the theory of localized heating in shear bands, followed by dissipation of the heat, allowing for recovery of the bulk material strength. In the second experiment, the response of Si was studied by dynamic x-ray diffraction. The crystal was observed to respond with uni-axial compression at a peak pressure 11.5-13.5 GPa.

INTRODUCTION

The dynamics of material response to pressure loading depends on the pressure and strain rate. Processes may be extremely slow, such as the movement of the tectonic plates on the earth (10^{-17}-10^{-14} s^{-1}) [1], or fast, such as the dynamic response of materials under shock loading (10^3-10^7 s^{-1} or higher) [2]. There are experimental techniques that allow us to access these different regimes. The diamond anvil cell is an example for slow isotropic compressions up to the 100 GPa range (limited by strength of the press itself). For dynamic processes, there are Hopkinson bar test facilities, gun facilities, and high explosive (HE) facilities. In these, the pressures are typically ≤100 GPa, and only moderate strain rates (10^3-10^6) are accessed. The response of a metal under extreme pressure (>100 GPa) and high strain rate (>10^7 s^{-1}) is typically inferred by extrapolation from experiments that are done at lower pressures (<100 GPa) and moderate strain rates (10^6 s^{-1}).

One model used to described material response under shock loading is the Steinberg-Guinan constitutive model [3]. This is a semi-empirical strain-rate independent model for the yield stress and shear stress:

$$Y(P,T) = Y_o \left[1 + \beta(\varepsilon + \varepsilon_i)\right]^n \left[1 + \left(\frac{Y_P^{'}}{Y_o}\right)\frac{P}{\eta^{1/3}} - \left(\frac{G_T^{'}}{G_o}\right)(T - 300)\right] \qquad (1a)$$

$$G(P,T) = G_o \left[1 + \left(\frac{G_P^{'}}{G_o}\right)\frac{P}{\eta^{1/3}} - \left(\frac{G_T^{'}}{G_o}\right)(T - 300)\right] \qquad (1b)$$

where the Y is the yield strength, G is the shear modulus, ε is the strain, and η is the compression. This model is an elastic-perfectly plastic model. When a stress is applied to a sample, it responds elastically up to the point where the stress exceeds the yield stress. At that point, it yields to plastic flow. This formulation includes the enhancement of strength due to pressure (P) and work hardening (β), and softening due to temperature (T).

In fact the material has a lattice structure that is not taken into account in such an empirical description. When the solid undergoes deformation at high pressure, stresses result in the generation and subsequent propagation of lattice dislocations [4]. Microscopically, solid state plastic flow is caused by the rearrangement of the lattice structure by transport of these dislocations.

The number density of dislocations that are generated and the speed with which they propagate are dependent on the rate of the applied strain. The parameters defined in the constitutive materials model are determined from experiments such as those with strain rates on the order of 10^3-10^6 s^{-1} [3]. Application of the model is speculative at the higher strain rates of 10^7-10^9 that may be achieved with a laser driven shock experiment. As a result, it is important to characterize the shock response of materials at such high strain rates.

Intense lasers have been used for high pressure fluid hydrodynamics experiments and EOS experiments relevant to ICF and to laboratory astrophysics. The laser provides a source of high energy density that may be used to launch shocks that are up to 10^5 GPa for fluid experiments. With appropriate target and laser pulse shape, materials may be compressed at more moderate pressures (>100 GPa) while remaining solid. This allows solid state experiments to be done in regimes of very high pressure and strain rate

In this paper we describe the experimental technique for performing solid state experiments using an intense laser. We present details of the target design, and drive characterization, along with calculations of the state of the material. We show results from RT instability experiments using thin Al foils, and we also discuss dynamic diffraction experiments probing the lattice response of shock compressed Si crystals.

ALUMINUM INSTABILITY EXPERIMENT

In a classical fluid model, when a light fluid accelerates a heavier fluid, the interface is Rayleigh-Taylor (RT) unstable. A mass modulation at the embedded material interface is unstable, and can grow when accelerated. In the solid state, however, the strength of the material can counter the effect of the RT instability. The parameters that define whether a material is stable or unstable to instability growth in the solid state depend on the wavelength and amplitude of the modulation, the acceleration, foil thickness, and material properties, such as yield stress, and shear modulus.

The effect of strength on instability growth in the plastic flow regime has been investigated by Barnes *et al* [5] using Al plates that have a pre-imposed surface modulation. The Al plates were driven with a shockless HE drive. Similar experiments were done by Lebedev *et al* [6, 7], using Al and Ti plates. We are conducting experiments on the Nova laser [8] to study the plastic flow of metals at high pressure and very high strain rates. Thin foils of Al are compressed by a factor of 1.5-2.0 with staged shocks reaching peak pressures of up to 180 GPa. The Rayleigh-Taylor instability is the observable "probe" in this experiment, with departures from classical (liquid) behavior characterizing the material strength properties at high pressure and compression.

In order to perform such a solid state experiment, the sample must be compressed nearly isentropically such that the final temperature is below the material melt temperature.

The Nova hydrodynamics experiments are conducted using an x-ray drive created in a cylindrical gold hohlraum. The target geometry is shown in Fig. 1. The hohlraum (Fig. 1a) is cylindrically symmetric, 3.44 mm in diameter, and 5.75 mm long. The hydrodynamics package is mounted on the side of the hohlraum at the midplane.

Eight Nova beams enter the hohlraum through the laser entrance holes and are incident on the inner wall of the two laser heated cavities of the target. The high intensity laser ionizes the surface of the hohlraum wall to create a plasma, and the laser energy is absorbed by inverse

Brehmsstrahlung. X-rays that are re-emitted from the wall pass through the holes in the internal shields to heat the central (x-ray heated) cavity and ablate material from the surface of the package. This launches a series of shocks to compress the package and accelerate it away from the hohlraum. The internal shields shown in Figure 1 prevent preheating of the package by hard x-rays generated at the laser spots.

The Al foil package consists of a 20 μm thick brominated polystyrene (CH(Br)) ablator pressed in contact with the Al foil (Fig. 1b). We typically use Al-6061 foils that have been rolled and then machined to have a sinusoidal modulation and an average thickness of 18-20 μm.

A purely isentropic compression may be achieved with a pressure pulse that rises slowly so that a shock cannot form in the material during the experiment. This is approximated in the laser experiment using two gentle shocks. An 8.5 ns long laser pulse shape is created by temporally staggering the 8 drive beams (Fig. 2). This generates an x-ray drive pressure that launches the two shocks to compress and accelerate the foil away from the side of the hohlraum.

We have characterized the x-ray drive in the central cavity of the hohlraum using the Dante diagnostic [9] and side-on foil trajectories. The Dante diagnostic is an array of absolutely calibrated filtered x-ray detectors. This provided a measurement of the radiation temperature as a function of time. We have also performed simulations of the drive inside the hohlraum to establish a detailed model for the drive history.

The peak portion and the late time decay of the drive are verified with side-on foil trajectory measurements of an Al foil. The Al foil moves approximately 140 μm after 20 ns. The drive history and calculated trajectory of the rear surface (free surface) of the Al foil is shown overlaid in Fig, 2.

The conditions in the Al foil are calculated at the embedded interface with the LASNEX 1-D hydrodynamics code [10]. The calculated temperature and pressure at the embedded ablator/Al interface are shown in Fig. 3. Two shocks are created, the first at a pressure of 200-300 kbar and the second at a pressure of 1.8 Mbar, as shown in Fig. 3a. The Atwood number is about 0.13 from 6-13 ns, and then it comes up to 0.2. The time-scale of this experiment is short, and the longitudinal strain rate is about 7×10^7 s^{-1}. The slow decay of the hohlraum x-ray drive maintains the high pressure until about 10 ns. During the experiment, the interface accelerates to a velocity of about 16 μm/ns at 20 ns. In these simulations, the material temperature at the interface stays below the melt temperature, which we calculate by the Lindemann law [described in 11]:

$$T_m = T_{mo} exp\{2a(1 - 1/\eta)\}\eta^{2(\gamma_o - a - 1/3)} \qquad (2)$$

where T_{mo} is the melt temperature at constant volume, η is the volume compression of the sample, γ is the Grüneisen gamma, and a is the coefficient of volume dependence of γ, as defined by Steinberg *et al.* [3]

This drive is calculated to keep the foil very near the conditions of an isentropic compression throughout the experiment. In Fig. 3b we show the internal energy at the Al interface plotted as a function of density (compression) from t=0 to t=15 ns. The dotted curve labeled "isentrope" here corresponds to an isentropic compression.

INSTABILITY GROWTH EXPERIMENTS

Sinusoidal modulations are machined in the Al foils with amplitudes of 0.5 μm, and wavelengths of 10, 20 and 50 μm. A 20 μm thickness of brominated plastic ablator is pressed onto the modulated foils, and then the package is mounted over a hole in the side of the

hohlraum. The x-ray drive ablatively launches a series of shocks to compress and accelerate the metal foil away from the side of the hohlraum.

Instability growth is diagnosed using x-rays that are generated by two additional beams on Nova which are incident on a separate metal backlighter foil. A large area (0.7 mm diameter) focal spot aligned to a separate Sc backlighter foil to generate He_α x-rays at 4.3 keV. Two-dimensional images of the x-ray transmission through the modulated foil is recorded using a gated x-ray imager (FXI). [12, 13]. Up to 16 images are recorded on 4 independently timed microchannel plate striplines on each laser shot, using a 230 ps wide gate pulse. A typical image is shown in Fig. 4, displayed in optical depth of the foil, normalized to the average. A lineout of the modulation in optical depth (Fig. 4b) is analyzed to extract the Fourier amplitude at the modulation wavelength. This is then normalized to the initial contrast in optical depth, and the instrument resolution is removed from the measurement. Note that the instrument modulation transfer function is about 0.6 at 12X for $\lambda=20$ μm.

The growth factors for $\lambda=10$, 20 and 50 μm modulations, with a 0.5 μm initial amplitude are shown in Fig. 5. Overlaid on the graphs, we have plotted the growth factors simulated using both a fluid model, and the constitutive material strength model described by Steinberg *et al*. The data show variation from shot to shot, but there is a clear trend. At about 15-16 ns, the growth factors are consistent with fluid growth. However, at later times (20-22 ns), the growth factors have not grown as much as we calculate using the fluid models. This suggests that there may be some saturation or stabilization of the instability growth. This is discussed below.

STRENGTH STABILIZATION

The initial value for yield strength of bulk Al-6061 is $Y_o=2.9\times10^{-3}$ Mbar and the initial value for shear modulus is $G_o=0.276$ Mbar. At a shock pressure of 1.8 Mbar, the Al foil is compressed by about a factor of 1.7-1.8, at which point the yield strength is 33 kbar, enhanced

by more than 10X over the nominal value, Y_o. The yield strength is exceeded by more than an order of magnitude, putting the foil into the plastic flow regime and allowing for instability growth in the solid state.

Estimates can be made as to whether the modulation on the Al package grows or not, based on a stability boundary analysis assuming steady-state conditions. Lebedev *et al* [6] provide an expression defining stability boundary as a function of both the amplitude and the wavelength of the modulation:

$$\eta_c = \eta_c(Drucker)\left[1 - 0.86e^{(2\pi H/\sqrt{3}\lambda)}\right]\left\{\left[1 - e^{(-2\pi H/\sqrt{3}\lambda)}\right]^2 - \left(\frac{\lambda}{\lambda_\infty}\right)^2\right\} \qquad (3)$$

where

$$\eta_c(Drucker) = \frac{2Y}{\rho g} \qquad (4)$$

is the wavelength independent critical amplitude threshold to instability growth from Drucker [14].

For the RT instability experiments, the stability curve is shown in Fig. 6. The initial amplitude is 0.5 µm, but under shock compression it is reduced to about 0.35 µm. For wavelengths $<\lambda=25$ µm, the growth is predicted to be stabilized, consistent with the simulations with strength. For longer wavelengths, it is predicted to grow. However, we observe growth that is fluid-like at early times for the 20 µm wavelength data, and then it stagnates.

One possible explanation for this behavior is that the foil is responding nearly fluid-like due to thermal softening in localized regions, and then it regains strength as the heat dissipates into the bulk material. This model is described by Grady and Asay [15]. As the energy stored in shear stress in the lattice dissipates in narrow regions (shear bands), large numbers of dislocations may be generated and the bulk sample may deform plastically. Grady and Asay have measured the size and spacing of shear bands observed in Al shock loading experiments

at strain rates up to 10^7 s^{-1}. The thermal dissipation time is on the order of 10 ns, consistent with the time scale over which we observe recovery of the strength in the RT instability experiments.

Although there is no explicit model to predict the response of a foil with shear band softening and subsequent recovery of strength, this scenario offers a qualitative explanation for the RT growth history. Results from the experiments presented here are similar to those of HE driven Al plate experiments described by Rayevsky *et al* [16]. There, when the plate experiences a shock loading, the perturbation growth is nearly fluid at early times, and it appears to saturate.

DYNAMIC X-RAY DIFFRACTION

In order to develop a full understanding of a solid state experiment such as the RT instability experiment described above, details of the response of the lattice are required. When the solid undergoes deformation at high pressure, stresses that occur at a lattice level result in the generation and subsequent propagation of dislocations [17] and localized shear bands. Plastic material flow is the rearrangement of the lattice structure by transport of these dislocations. The number density of dislocations that are generated and the speed with which they propagate are dependent on the rate of the applied strain.

The technique of Bragg x-ray diffraction is being developed as a diagnostic for laser driven solid state experiments [18-21]. This technique provides a time-resolved measurement of the 2d lattice spacing. Here, x-rays scattered from the atoms in the lattice constructively interfere when the incident angle with respect to the lattice plane satisfies the Bragg condition:

$$n\lambda = 2d \times \sin(\theta) \tag{5}$$

The x-rays are diffracted at an angle θ equal to the incident angle (relative to the lattice planes) (Fig. 7).

When the lattice undergoes a deformation due to shock compression, the lattice compresses, so the lattice spacing decreases. The Bragg diffraction condition is then met at a different angle determined by the new lattice spacing, provided the x-ray source is close enough to the sample that the crystal subtends a large enough range of angles to include the new Bragg angle. The shift in diffraction angle is recorded as a spatial shift in the diffraction signal.

Since the x-rays that are typically used for Bragg diffraction are multi-keV, the depth in the crystal that can be probed may be 10s of microns. If there is a range of densities and corresponding lattice spacings within this depth of the surface, we record a Bragg diffracted signal from the corresponding range of angles. In other words, we record a measure of the fraction of the material that is compressed at each density. For the case where there is a shock wave with a monotonic pressure profile (which results in a monotonic variation in material density for the case where there are no volumetric changes associated with a phase transition), the dependence of the diffraction signal on compression in principle can provide a measurement of the shock wave profile [22].

Previously, dynamic x-ray diffraction has been done on laser driven LiF and Si crystals [19, 23]. Additional experiments have been done with KCl and LiF shock compressed with an impactor on a powder gun facility [24, 25]. We have done experiments to study shock compressed single crystal Si as a way to develop the technique for our laser experiments with the goal of characterizing the lattice response of the shocked Al samples used for RT instability experiments.

Up to 8 beams of Nova are incident in the cylindrical gold hohlraum target shown in Fig. 1a to generate a Planckian soft x-ray drive. A Si crystal sample is mounted over the hole in

the side of the hohlraum at the midplane. The crystal is 1 x 2 mm in size and 40 μm thick. It was cut for different experiments with a (111) or (100) orientation.

A 4 ns square laser pulse shape is used to drive a single shock in the Si. Two additional beams of Nova are used to generate the x-ray source for Bragg diffraction. These beams are pointed onto a thin V or Fe foil (5 μm) that was masked with a Ta pinhole aperture (Fig. 3) to provide a small (100 μm) source of K-shell line emission. The emission from this backlighter source is self filtered by the foil itself to provide a nearly mono-energetic backlighter spectrum.

The backlighter foil is located close to the crystal so that the crystal subtends an angle of up to about 25° to the x-ray source, allowing for a range of Bragg diffraction angles. The x-rays diffracted from the crystal are recorded with an x-ray streak camera. This camera is located with the photocathode only 12 cm from the target in order to collect nearly a 15° range of diffraction angles from the target. A film holder is located in front of the streak camera to record a time-integrated record of the diffracted x-rays as well as the streak record. A second film holder was located on the opposite side to record the x-rays diffracted from the orthogonal lattice planes ((040) lattice planes) in the case of the Si (100) shock experiments (Fig. 8).

DRIVE SCALING OF Si (111)

Silicon at ambient pressure is a diamond cubic lattice. The 2d spacing for the (111) lattice planes is 6.27 Å. The Bragg angle for V x-rays at 2.38 Å is 22.3°. We recorded the diffracted signal from the (111) lattice planes at a range of drive pressures from 13to 32 Gpa, above the HEL for Si (111), which is 5.4 GPa. Figure 9 shows the time-resolved diffraction signal recorded from the free surface of Si (111) shock compressed to (a) 13 GPa and (b) 32 GPa. These streaks are labeled to indicate compression as a function of time.

The streak records shows a diffraction peak corresponding to the nominal lattice spacing up. An additional diffraction peak corresponding to the compressed lattice is visible up until the time the shock reaches the free surface, at which point the crystal is fully compressed and the static diffraction peak disappears. At shock breakout, the lattice releases, and the diffraction pattern shows an intermediate compression due to the dynamics of the release and a return to the initial (unshocked) lattice spacing.

We are able to reproduce many of the features in the diffraction pattern using the LASNEX hydrodynamics code. This is illustrated in Figure 10, where we show a plot of axial elastic strain, displayed as a function of time for the case of Si (111) shocked to a peak pressure of 13 GPa. This shows the diffraction from the unshocked and shocked lattice, as well as the appearance of intermediate compression as the material releases. This simulation also shows a diffraction peak due to the elastic precursor wave, which we do not observe in the experiment. Such a simulation does not include the presence of the lattice and associated lattice dynamics. Molecular dynamics simulations are required to provide more insight into the lattice response. [26, 27]

MEASUREMENTS OF ORTHOGONAL PLANES OF SILICON (100)

An Fe backlighter foil provided He_ x-rays of wavelength 1.85 Å, which diffract from the uncompressed (400) lattice planes at a Bragg angle of 42.95°. The crystal was shocked along the (400) direction, and we recorded diffracted x-rays from the (400) (Bragg) and (040) (Laue) lattice planes simultaneously (Fig. 8). In Figure 11 we show the data from two separate Nova shots. In the first case (Fig. 11a), we recorded the Bragg diffraction on static film (integrated over the duration of the backlighter pulse) and an x-ray streak camera. The Laue diffraction was recorded only on static x-ray film. For the second shot (Fig 11b), the Laue diffraction was recorded with the streak camera.

The Bragg diffraction signal shows 2 strong peaks. One corresponds to diffraction from the uncompressed lattice. This is labeled to indicate fractional 1-D compression normalized to the initial (111) lattice spacing as a function of time. We observe diffraction from the uncompressed Si, and also from shock compressed Si as the shock propagates toward the free surface of the crystal. The lattice is compressed in the shock direction by 6%. As the shock breaks out at the back surface, the crystal is fully compressed and the signal from the unshocked material disappears. The rarefaction returns the crystal to the initial density, characterized by the return of the diffraction signal corresponding to solid density Si.

The Laue signal recorded over the full extent of the Bragg streak shows only a single peak, suggesting that there is no transverse compression. The time-resolved Laue signal is shown in Fig. 11b. There is no change in the Laue signal as a function of time, through the time of shock breakout, suggesting that the Si lattice responds uni-axially on the time scale of the experiment (nanoseconds). Note that in this case, the time-integrated Bragg signal shows the same two peaks, one corresponding to standard Si, the second to shock compressed Si.

SUMMARY

We have demonstrated that high pressure and strain rate solid state experiments may be done using an intense laser. By introducing internal shielding in the hohlraum target to prevent x-ray preheat and by shaping the laser pulse to generate a sequence of shocks, a metal foil may be compressed nearly isentropically. A RT instability experiment was conducted using thin Al foils with a pre-imposed modulation at the unstable embedded interface. Measured growth rates are suggestive of the shock response model of localized heating in shear bands that dissipates, after which the material recovers strength. A dynamic diffraction experiment was also performed using Si crystals. Silicon crystals were shocked along the (111) lattice direction

at up to 33 GPa. Additionally, Si (400) was shocked at 11.5-13.5 GPa. Only a 1-D compression was observed, indicating that the response is purely elastic on the ns time scale.

ACKNOWLEDGMENTS

REFERENCES

[1] P. England, and P. Molnar, Science **278**, 647 (1997).

[2] example summary in D. J. Steinberg and C. M. Lund, J. Appl. Phys. **65**, 1528 (1989).

[3] D. J. Steinberg, S. G. Cochran, M. W. Guinan, J. Appl. Phys. **51**, 1498 (1980).

[4] L. C. Chhabildas, J. R. Asay, J. Appl. Phys. **50**, 2749 (1979).

[5] J. F. Barnes, P. J. Blewett, R. G. McQueen, K. A. Meyer, D. Venable, J. Appl. Phys. **45**, 727 (1974).

[6] A. I. Lebedev, P. N. Nizovtsev, V. A. Rayevsky, in the Proceedings of the 4th International Workshop on the Physics of Compressible Turbulent Mixing, 29 March - 1 April, Cambridge, England (Cambridge University Press, 1993), p. 81.

[7] A. I. Lebedev, P. N. Nizovtsev, V. A. Rayevsky, V. P. Soloviov, in the Proceedings of the 6th International Workshop on the Physics of Compressible Turbulent Mixing, 17-21 June, 1997, Marseille, France (I.U.S.T.I./C.N.R.S., Marseille, 1997).

[8] E. M. Campbell, J. T. Hunt, E. S. Bliss, D. R. Speck, R. P. Drake, Rev. Sci. Instrum. **57**, 2101 (1986).

[9] H. N. Kornblum, R. L. Kauffman, J.A. Smith, Rev. Sci. Instrum. **57**, 2179 (1986).

[10] G. B. Zimmerman and W. L. Kruer, Comments Plasma Phys. Control. Fusion **2**, 51 (1975).

[11] Lindemann melt curve

[12] P. M. Bell, J. D. Kilkenny, G. Power, R. Bonner, D. K. Bradley, in Ultrahigh Speed and High Speed Photography, Photonics, and Videography '89 (SPIE, Bellingham, WA, 1989), Proc. SPIE Vol. 1155, pp. 430-444.

[13] K. S. Budil, *et al*, Rev. Sci. Instrum. **67**, 485 (1996).

[14] D. C. Drucker, Ingenieur-Archiv **49**, 361 (1980).

[15] D. E. Grady and J. R. Asay, J. Appl. Phys. **53**, 7350 (1982).

[16] V. Rayevsky, A. Lebedev, A. Michailov, P. Nizovtsev, S. Sinitsina, V. Soloviov, V. Ogordnikov, to appear in the Proceedings of the 8th International Workshop on the Physics of Compressible Turbulent Mixing, 4-7 July, 1999, St. Petersburg, Russia.

[17] E. Zaretzky, J. Appl. Phys. **78**, 1 (1995).

[18] Q. Johnson, , A. Mitchell, R. N. Keeler, L. Evans, Phys. Rev. Letters **25**, 1099 (1970); Q. Johnson, A. Mitchell, L. Evans, Nature **231**, 310 (1971).

[19] J. S. Wark *et al*, Phys. Rev. B **40**, 5705 (1989).

[20] A. A. Hauer *et al*, Proc. SPIE **3157**, 72 (1997).

[21] D. H. Kalantar, *et a;*, Rev. Sci. Instrum. **70**, 29 (1999).

[22] N. C. Woolsey and J. S. Wark, J. Appl. Phys. **81**, 3023 (1997).

[23] N. C. Woolsey, J. S. Wark, D. Riley, J. Appl. Crystallogr. **23**, 441 (1990).

[24] E. Zaretsky *et al*, Sov. Phys. Dokl. **36**, 76 (1991).

[25] P. Riggs

[26] B. L. Holian and P. S. Lomdahl, Science, 1998.

[27] J. Belak

a) Hohlraum target

backlighter foil

x-ray heated cavity

backlighter beam

internal shield

Nova drive beam

x-rays

axis

laser entrance hole

laser heated cavity

x-ray drive

CH(Br), Al package

b) Rayleigh-Taylor package

brominated plastic

x-ray drive

0.5 μm

20 μm

19 μm

50 μm

Al foil
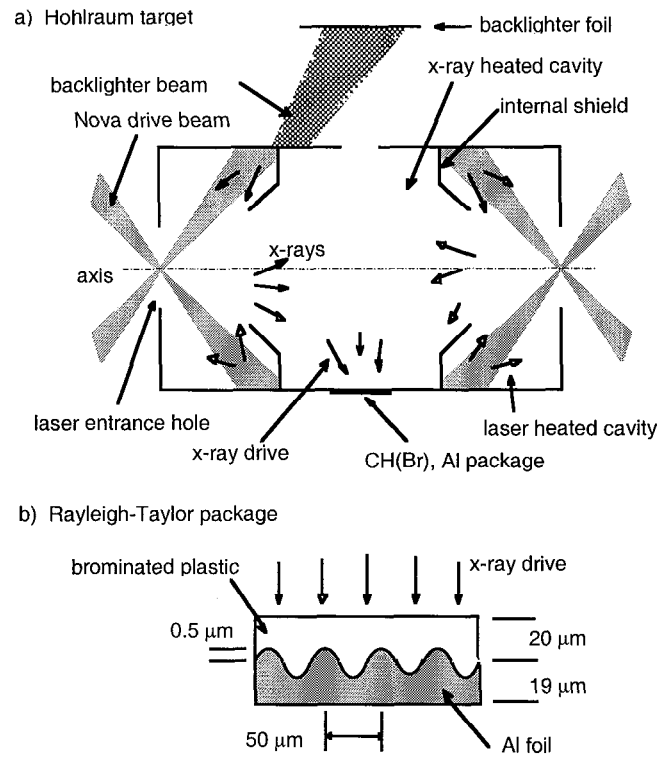
Figure 1: a) Hohlraum target configuration showing the laser heated cavities, the x-ray heated cavity, and the internal shields to block x-ray preheating of the foil package. b) Cross-section of a typical RT instability package consisting of a CH(Br) ablator and modulated Al foil.
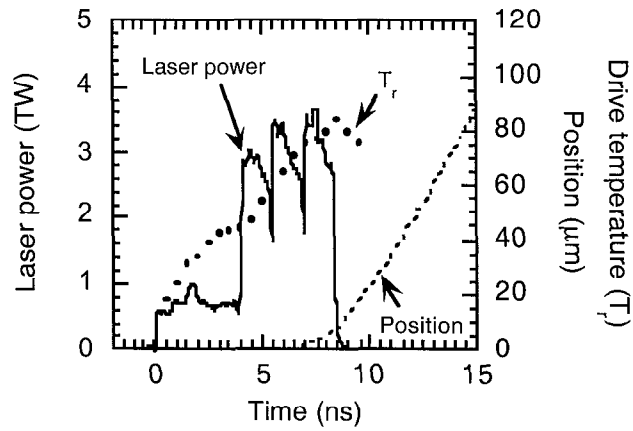
Figure 2: Laser pulse shape used, resulting x-ray drive temperature and simulated foil trajectory
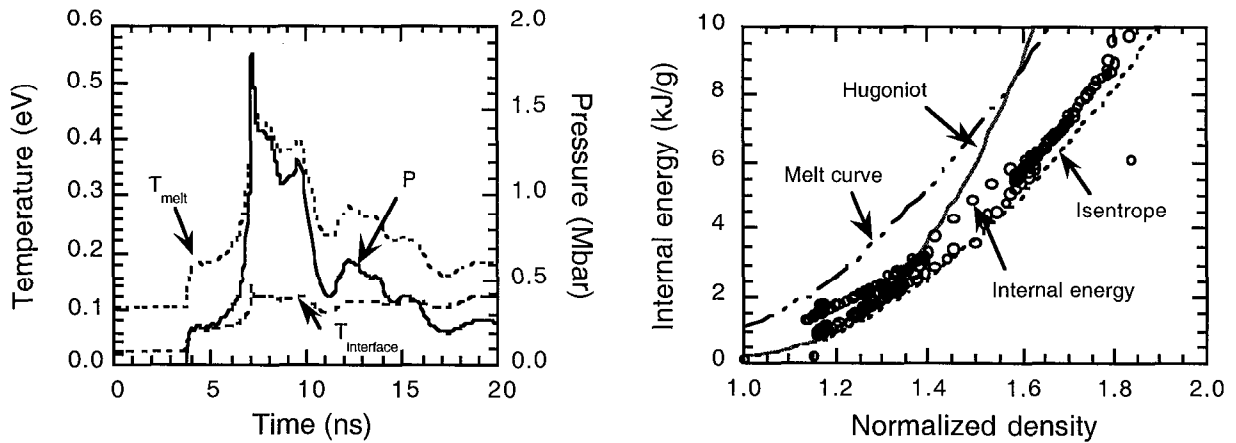
Figure 3: a) Pressure and temperature history at the embedded interface for a shocked Al foil. The melt temperature calculated by the Lindemann melt law is overlaid. b) Internal energy trajectory calculated for the embedded Al interface. This is shown with the melt curve, shock hugoniot, and an isentrope.
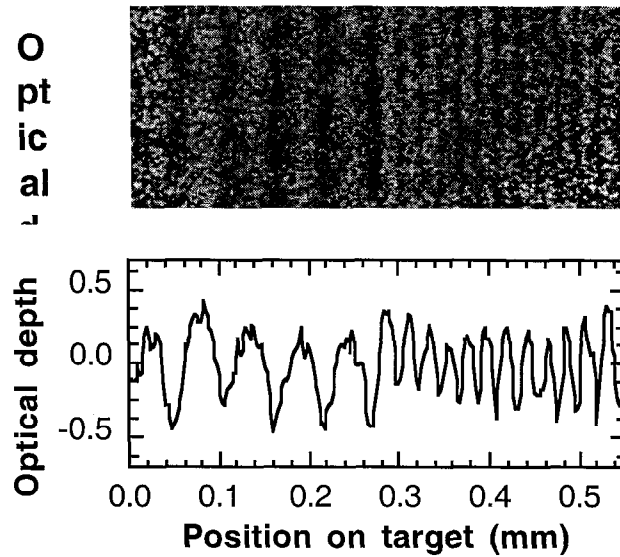
Figure 4: a) Sample x-ray radiograph of a 50 µm wavelength perturbation. This is shown as modulation in optical depth for the 4.3 keV probe x-rays. b) Lineout of optical depth modulation.
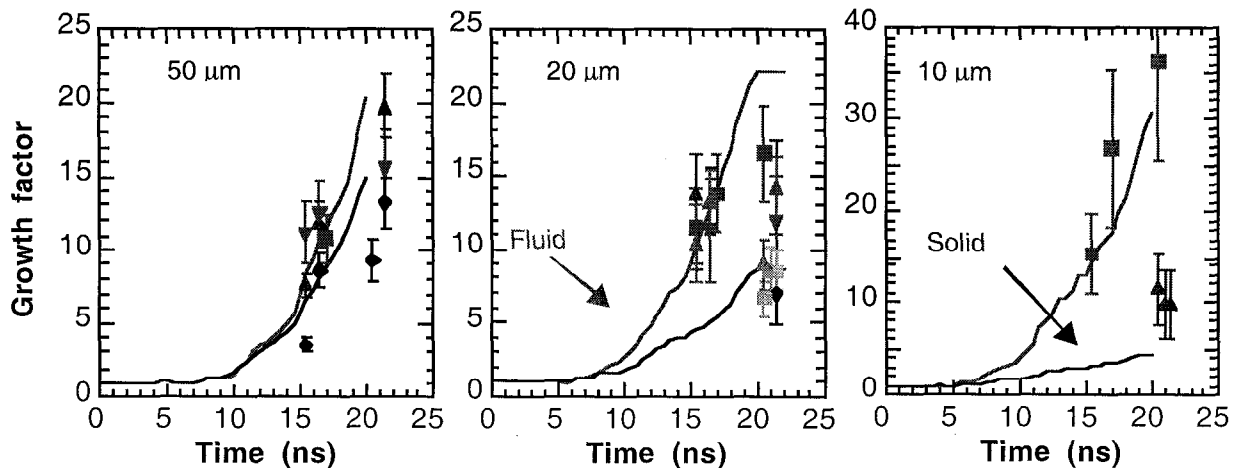
Figure 5: Measured growth factors for the Al RT instability experiments: a) 50 µm modulation, b) 20 µm modulation, and c) 10 µm modulation.
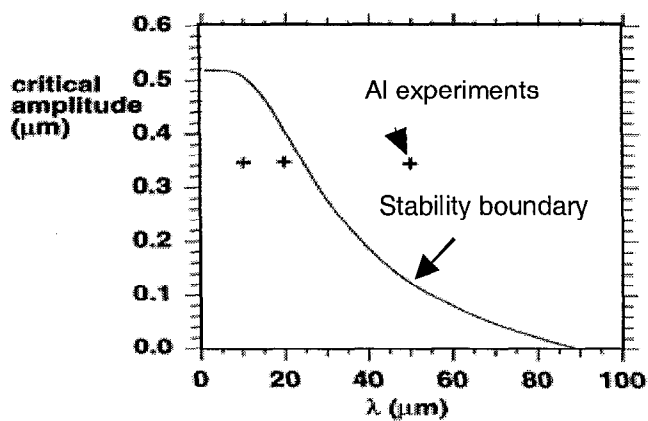
Figure 6: Stability boundary calculated with the Lebedev formulation for the Al RT instability experiment.
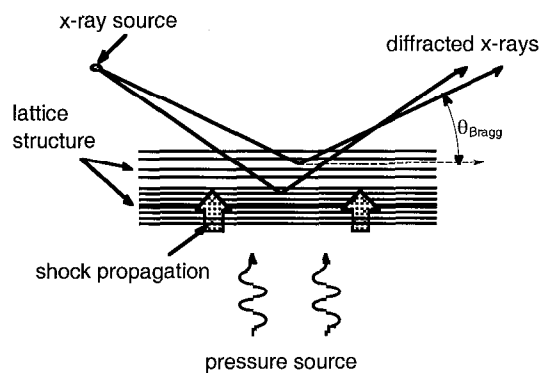
Figure 7: Illustration of dynamic x-ray diffraction being applied to probe lattice compression of a shocked sample.
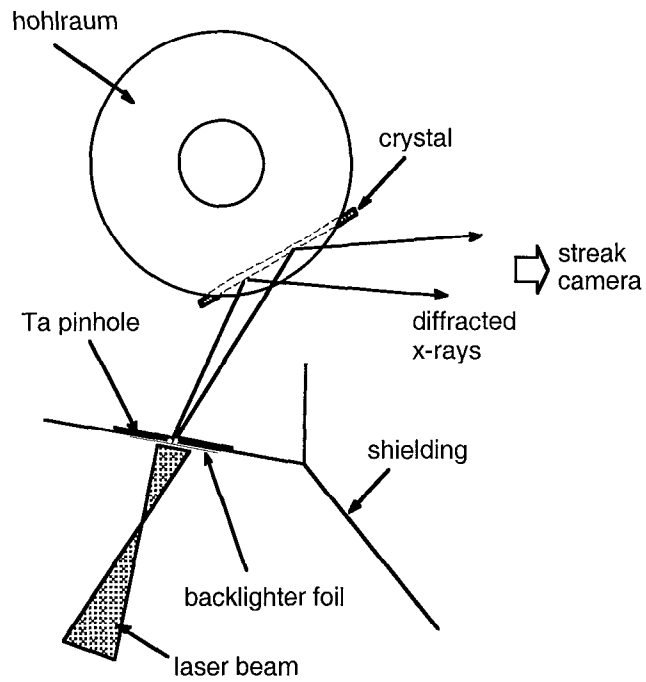
Figure 8: Diagram of the hohlraum target configuration for dynamic x-ray diffraction measurements.
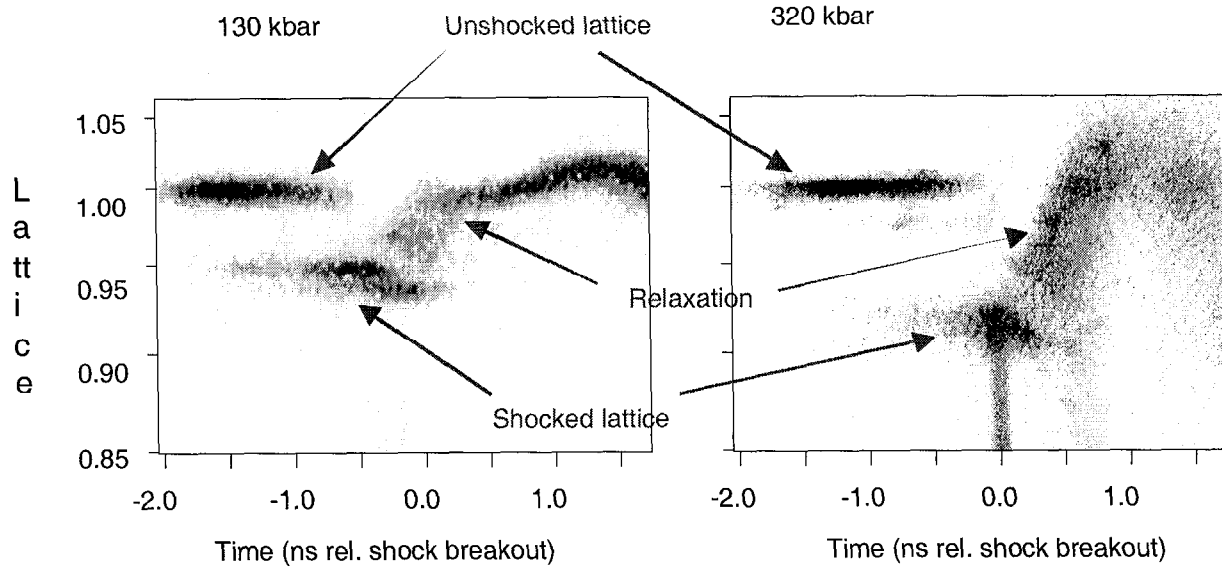
Figure 9: Time-resolved x-ray diffraction data recorded from shock compressed Si (111) at pressures of (a) 13 GPa and (b) 32 GPa.
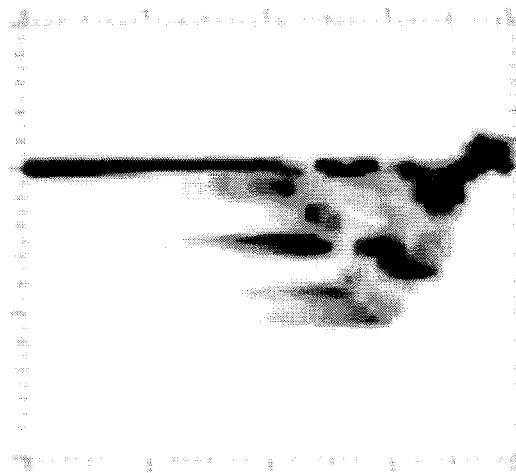
Figure 10: Simulated x-ray diffraction from Si (111) shock compressed to 13 GPa.
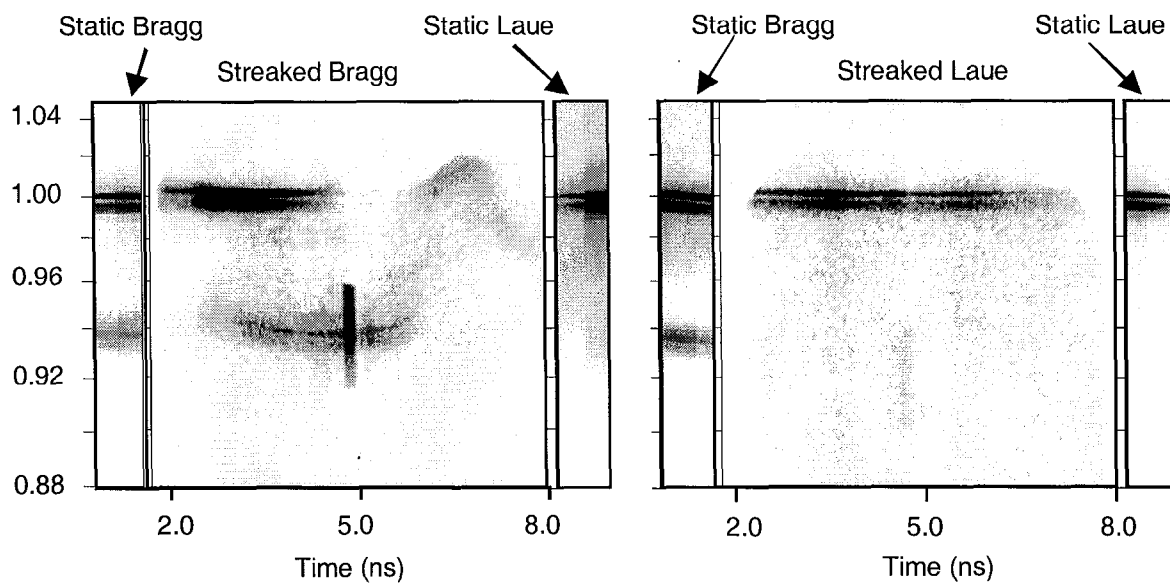
Figure 11: Time-integrated and time-resolved data showing simultaneous diffraction from (400) and (040) lattice planes in Si shocked along the (400) direction at 11.5-13.5 GPa.

LIST OF FIGURES

9. Time-resolved x-ray diffraction data recorded from shock compressed Si (111) at pressures of (a) 13 GPa and (b) 32 GPa.

10. Simulated x-ray diffraction from Si (111) shock compressed to 13 GPa.

11. Time-integrated and time-resolved data showing simultaneous diffraction from (400) and (040) lattice planes in Si shocked along the (400) direction at 11.5-13.5 GPa.